Proceedings of the ASME 2023
International Design Engineering Technical Conferences &
Computers and Information in Engineering Conference
IDETC/CIE 2023
August 20-23, 2023, Boston, Massachusetts,

DETC2023-116489

TOPOLOGICAL INSULATOR-BASED ELECTROACOUSTIC TRANSISTORS

Sai Aditya Raman Kuchibhatla and Michael J. Leamy*

G. W. Woodruff School of Mechanical Engineering
Georgia Insitute of Technology
Atlanta, Georgia, 30332
E-mail: michael.leamy@me.gatech.edu

ABSTRACT

We propose an electroacoustic transistor enabled by reconfigurable topological insulators (TIs). The underlying structure of the device is a hexagonal lattice with a unit cell consisting of piezoelectric disks bonded to an aluminum substrate. First, we study the dispersion of flexural waves in the reconfigurable TI to identify Dirac cones in the band structure of a unit cell possessing C_{6v}-symmetry. A topological bandgap can be opened by breaking inversion symmetry in the unit cell. This is achieved by altering the elastic response of one of the affixed piezoelectric disks using a negative impedance shunt circuit. Next, we analyze various topological states formed by interfacing mirror-symmetric unit cells. Sublattices with interface states are then combined to construct a transistor supercell which hosts at least two topologically protected channels for wave propagation. The amplitude of an incoming acoustic signal propagating in one of the topological channels, referred to as the 'Gate', is used to switch on or off a second topological channel between a wave source and receiver, mimicking the behavior of a field effect transistor in electronics. We employ finite element analysis to study the harmonic response of the transistor structure demonstrating the OFF and ON states of the device. Further, we present a mock-up of an electrical circuit which enables the switching of the topological channel between a wave source and receiver. The design of the proposed wave-based transistor promises the advantage of topological protection and may find applications in wearable devices, edge computing, and sensing in harsh environments.

NOMENCLATURE

- a Unit cell length.
- α Ratio of negative capacitance to the capacitance of piezoelectric disk.
- C_0 Capacitance in the feedback loop of shunt circuit.
- C_p Capacitance of piezoelectric disk.
- C_{neg} Effective negative capacitance of shunt circuit.
- k_{31} Piezoelectric electromechanical coefficient.
- p Polarization of eigenmode.
- R_0 Bias resistance.
- R_1, R_2 Resistors used in shunt circuit.
- u displacement in x-direction.
- v displacement in y-direction.
- V volume of the unit cell.
- w displacement in z-direction.
- x Coordinate along the length of the structure
- y Coordinate along the width of the structure
- z Coordinate perpendicular to the plane of the structure (thickness direction).
- Y_0 Short circuit modulus of piezoelectric disk.
- Y Shunted modulus of piezoelectric disk.

*Address all correspondence to this author.

INTRODUCTION

Recent need for low-power high-speed computing solutions for applications such as the Internet of Things (IoT) and wearable electronics has led to a renewed interest in practical acoustic and mechanical logic devices [1]. Of particular interest are devices which can perform logical operations while being an integral part of a structure or robot deployed at the end of a network or perhaps in extreme environments [2, 3]. Acoustic/mechanical logic devices operate continuously and can handle analog input signals better while avoiding the need for analog-to-digital converters. Further, by adding an electrical degree of freedom, these mechanical devices can replace or augment existing electronics to produce hybrid technologies with improved speed, performance and energy efficiency.

The basis of computing is a functionally complete set of logic gates which can be used to construct any truth table. For example, AND and NOT are one set of functionally complete logic gates. Some of the recent research efforts in the area of mechanical computing are aimed at developing such logic gates based on multistable soft structures [4, 5] and mechanical metamaterials [6,7]. Other hybrid approaches have used conductive mechanical materials [8,9], microelectromechanical systems (MEMS) or nanoelectromechanical systems (NEMS) [10, 11] to leverage electrical stimuli/response as an extra degree of freedom appended to the mechanical system. A major advantage of mechanical logic gates is that these devices utilize mechanical energy and have small to no electromagnetic signature. These can process information through mechanical interactions and store digital data without requiring electrical power. However, recently proposed mechanical logic devices suffer from one or more limitations such as functional-incompleteness (i.e. one or more truth tables can not be constructed), inability to return to their original state, and lack of reconfigurability. For the designs which overcome such limitations, speed and scalability are significant challenges which need to be addressed to realize practically useful implementations.

Researchers have also explored wave-based platforms to achieve boolean logic. In the past decade, acoustic logic gates have been proposed using phase modulation [12], self-collimated beams [13], density-near-zero metamaterials [14] and nonlinearity in granular media [15]. A need for different underlying mechanical structure for each gate and lack of reconfigurability are some of the major limitations of these approaches. Incorporating electrical stimulus into the acoustic systems is one way to enable reconfigurability. Researchers have demonstrated electrically tunable acoustic metamaterials [16–18] which may be leveraged to develop electroacoustic logic.

Topological acoustics has attracted attention in recent years owing to the robustness of edge and interface modes exhibiting scattering-free wave propagation. First identified as electronic states in condensed matter [19, 20], such phenomena have now been established in photonic [21], classical electromagnetic [22] and acoustic media [23–25]. Topological edge modes found in acoustics are analogs of quantum effects such as the quantum Hall effect (QHE) [26], quantum spin Hall effect (QSHE) [27] or quantum valley Hall effect (QVHE) [28]. While the quantum Hall effect requires breaking time reversal symmetry in the system, the other two only require spatial inversion symmetry to be broken. Amongst the three, QVHE-analogs are the simplest to achieve as they do not require external bias, like QHE-analogs, or strong coupling of modes, like QSHE-analogs.

A valley Hall topological insulator (VHTI) is designed by first identifying a unit cell with mirror symmetry (termed spatial inversion symmetry or SIS) possessing Dirac cones in its band structure. Then, mirror symmetry is broken to open a topological bandgap at the vertex of the Dirac cone. At frequencies within the gap, topologically protected waves propagate along an interface with mirrored SIS-broken unit cells on either side. QVHE was first predicted in graphene [29] and subsequently observed in solid-state devices [28, 30]. VHTIs have also been demonstrated using photonic [31, 32] and phononic metamaterials [33–35]. More recently, QVHE-based reconfigurable topological insulators [36] have been demonstrated which allow for modification of wave propagation paths within the structure. VHTIs can be miniaturized to manipulate elastic waves on chips [37] and tailored to perform operations such as multiplexing [38]. Thus, topological insulators are attractive candidates for acoustic logic devices [39] offering the advantage of scattering-free lossless wave propagation through topological channels.

In this work, we propose an electroacoustic transistor by leveraging switchable states in a reconfigurable topological insulator. The electroacoustic transistor mimicks the function of a field effect transistor (FET) in electronics where an input voltage at a 'gate' terminal enables a current flow between a 'source' and a 'drain' terminal. Figure 1(a) illustrates the idea of an electroacoustic transistor where an incoming wave of energy above a threshold value at the gate terminal opens a wave propagation channel between a wave source and receiver (referred to as drain in analogy with electronics). The proposed transistor offers two stable states (ON and OFF). Multiple instances of the transistor can combine to form logic gates, similar to digital electronics and may find several applications to include sensors for harsh environments, analog acoustic computers for edge computing in IoT networks, and multiplexers and demultiplexers in next-generation communication. We organize the paper as follows - first, we describe the unit cell of the reconfigurable topological insulator lattice and present its band structure wherein we identify a topological bandgap for flexural waves. Then, we interface mirrored versions of the symmetry-broken unit cell and show the presence of energy localized states within the topological gap. Next, we construct a transistor supercell by combining suitable interfaces and discuss a method to switch one interface based on wave energy in the other. Finally, we demonstrate the binary states in the transistor and conclude with some remarks on ex-

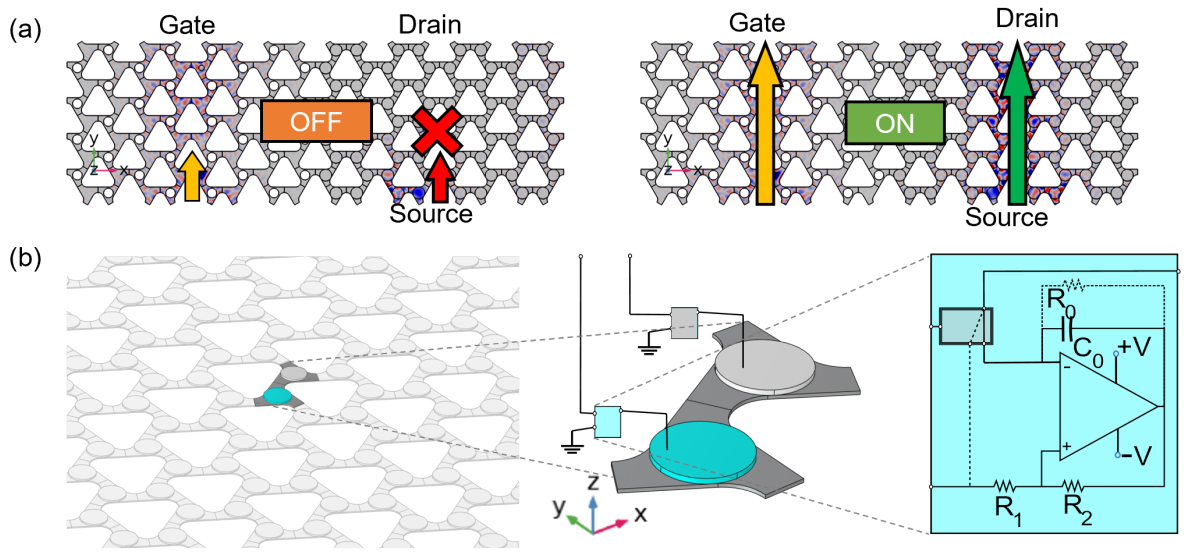

FIGURE 1. (a) ILLUSTRATION OF THE ELECTROACOUSTIC TRANSISTOR IN OFF (LEFT) AND ON (RIGHT) STATES. (b) UNIT CELL OF THE RECONFIGURABLE TOPOLOGICAL INSULATOR WITH NEGATIVE CAPACITANCE SHUNT CIRCUIT. CYAN DISKS ARE SHUNTED WHILE GREY DISKS ARE SHORT CIRCUITED RESULTING IN ASYMMETRY IN THE UNIT CELL.

perimental validation.

RECONFIGURABLE TOPOLOGICAL INSULATOR UNIT CELL

The reconfigurable topological insulator which forms the basis of the proposed electroacoustic transistor is a hexagonal lattice with a unit cell consisting of piezoelectric disks attached to an aluminum substrate as depicted in Fig. 1(b). We consider an aluminum plate of 0.635 mm (0.025") thickness and lead zirconate titanate (PZT) disks of 15 mm diameter and 0.9 mm thickness. Typically, a thin layer of epoxy adhesive is used to vacuum bond the piezo disks to the substrate enabling an accurate transmission of displacement between them. The unit cell distance is $a = 0.045$ m and the specific geometry is obtained by maximizing the area overlap between the host and piezoelectric disks. Shunting of piezoelectric materials is known to vary their elastic response and has been studied as a means to damp vibrations [40–42]. Specifically, the negative capacitance circuit shown in the Fig. 1(b) consists of an operational amplifier, a capacitor C_0, and resistors R_0, R_1 and R_2, and is used to reduce the effective elastic modulus [43, 44]. The circuitry results in an effective negative capacitance $C_{neg} = -C_0R_2/R_1$ connected to the piezoelectric disks. For stable implementation of the circuit, the disk capacitance C_p should be less than the magnitude of C_{neg}. The bias resistor R_0 also serves to keep the circuit stable at high frequencies. The effective modulus of elasticity of a shunted piezo is obtained, following [43], as

$$Y = Y_0 \left[1 - \frac{k_{31}^2}{(1+\alpha)}\right]^{-1} \tag{1}$$

where Y_0 is the short circuit Young's modulus of the piezo disk, k_{31} is the electromechanical coupling coefficient [42] of the piezo disk and $\alpha = C_{neg}/C_p$ is the ratio of negative capacitance to the unloaded disk capacitance. With $k_{31} = 0.37$ and $C_p = 3.5$ nF for the piezo disk (STEMiNC part no. SMD15T09S411) considered in the design of our unit cell, we obtain a shunted modulus $Y = 45$ GPa for $\alpha = -1.2$. The required $C_{neg} = -5.6$ nF can be constructed with any combination of the passive components of the NC circuits. For instance, $C_0 = 1.6$ nF, $R_1 = 1$ kΩ and $R_2 = 3.5$ kΩ can be used for this purpose.

In order to compute the band structure, we solve the eigenvalue problem formulated by applying Floquet-Bloch boundary condition to a single unit cell, using a commercial Finite Element (FE) package [45]. We use effective properties of the piezoelectric disks, thereby avoiding electrical degrees of freedom and exclude the negligibly thin adhesive layer to reduce the overall computational cost. For the inversion symmetric unit cell we consider an elastic modulus which is the average of the short circuited and shunted elastic modulus, such that one half of the unit cell is softened while the other is stiffened to break SIS. The material properties used in the numerical simulations reported in this paper are listed in Table 1. Figure 2(a) depicts the band struc-

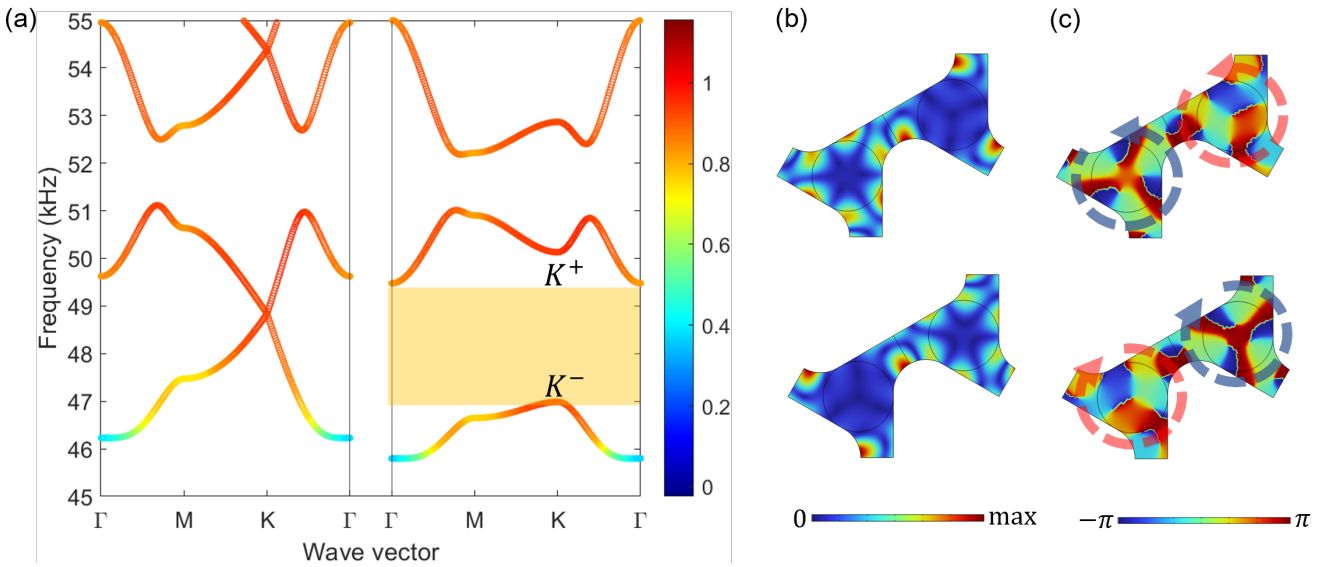

FIGURE 2. (a) PHONONIC BAND STRUCTURE OF THE RECONFIGURABLE UNIT CELL WITH (LEFT) AND WITHOUT (RIGHT) INVERSION SYMMETRY. (b) MAGNITUDE AND (c) PHASE OF THE z-DISPLACEMENT FIELD ACROSS THE UNIT CELL AT K^+ (TOP) AND K^- (BOTTOM) POINTS MARKED IN (a) .

ture of the reconfigurable unit cell with (left) and without (right) inversion symmetry. The colorbar indicates the polarization of the mode which is computed as

$$p = \frac{1}{V}\iiint \frac{w^2}{u^2+v^2+w^2} dV \tag{2}$$

where u,v, and w are the x-,y-, and z-displacements, respectively, and the integral is over the volume (V) of the unit cell. A value of polarization closer to 1 suggests a flexural mode. A gap around 48 kHz can be noted in the band structure. The frequencies surrounding the gap at the K-point are marked as K^+ and K^- in the band structure of the symmetry-broken unit cell in Fig. 2(a). The magnitude and phase of the z-displacement field in the unit cell at K^+ (top) and K^- (bottom) are shown in Fig. 2(b) and (c), respectively. The direction of increasing phase in Fig. 2(c), identified using the colormap, is counter-clockwise and clockwise at K^+ and K^- points, respectively. The difference in the direction of the phase flow is indicative of the topological nature of the gap [46]. Interfacing two lattices made of mirrored SIS-broken unit cells results in a structure which hosts topologically protected states within the gap. We consider various interface states which can be obtained with the reconfigurable unit cell in the next section.

TRANSISTOR SUPERCELL ANALYSIS

VHTI can host interface states of the armchair, bridge or zigzag type [47]. In this work, we consider the bridge and zigzag

TABLE 1. MATERIAL PROPERTIES USED IN STRUCTURAL FINITE ELEMENT STUDIES.

Material	Young's Modulus (GPa)	Density (kg/m^3)	Poisson's Ratio
Aluminum	69	2700	0.33
PZT Shorted	74	7800	0.31
PZT Shunted	46	7800	0.31

type interfaces which can be formed by neighboring shunted or shorted piezoelectric disks. We construct supercells by interfacing sublattices produced by repeating mirrored unit cells along one of the lattice vectors. We assume the supercell is infinitely periodic in the second lattice vector direction, as shown in Fig. 3. Applying Floquet-Bloch boundary condition and solving the eigenvalue problem produces the band structure of the supercell. The interface modes are confirmed by visual inspection of the displacement localization in the states found in the highlighted frequency region in Fig. 3. The bridge type interface with neighboring shorted piezos (referred to as Type A), does not host any topological interface modes while that with shunted piezos (referred to as Type B) hosts an interface state. In the zigzag case, both the interface with shunted neighbor (Type C)

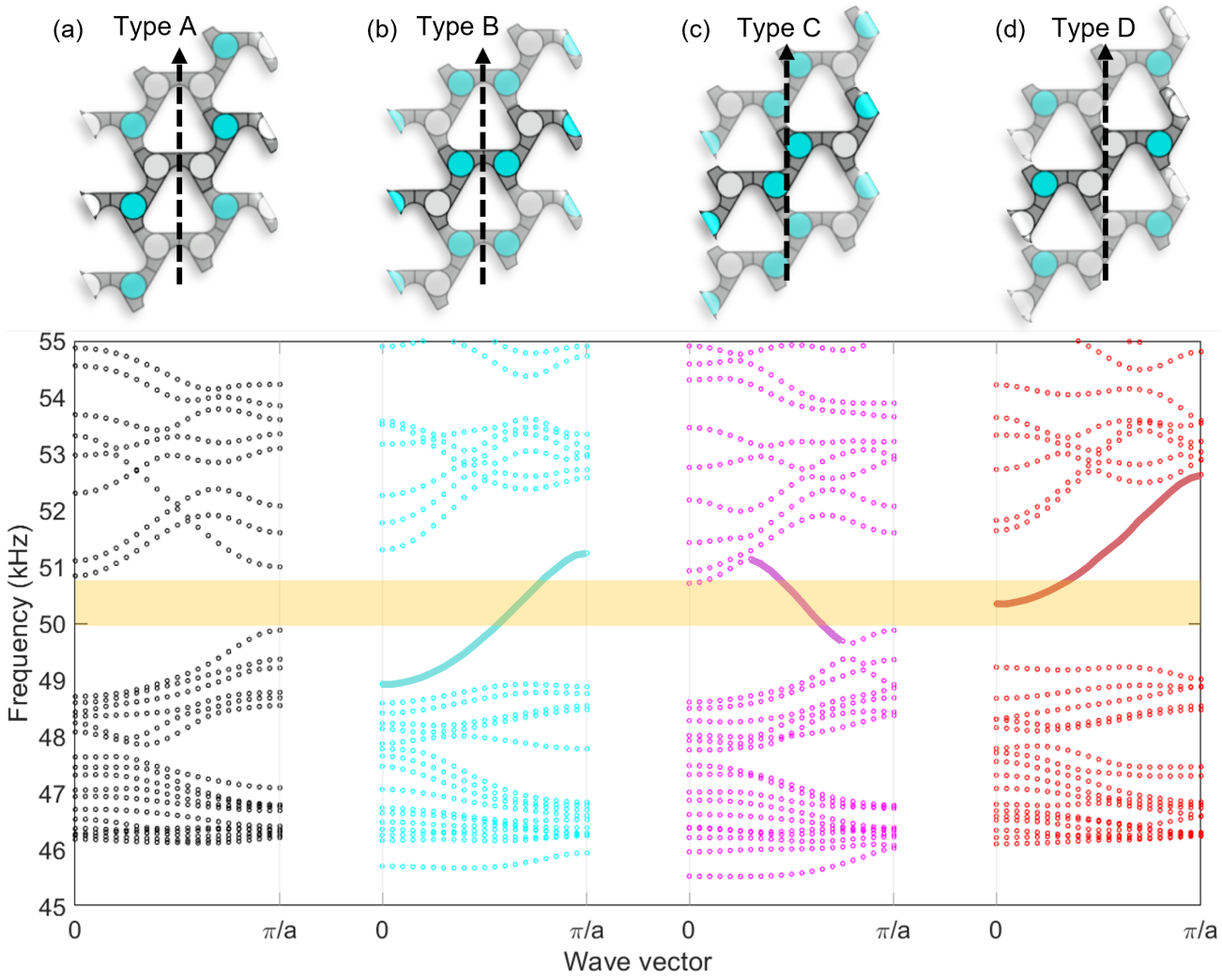

FIGURE 3. BAND STRUCTURE OF SUPERCELLS WITH BRIDGE (a,b) AND ZIGZAG (c,d) TYPE INTERFACES FORMED BY NEIGHBORING SHORTED (a,d) AND SHUNTED (b,c) PIEZOELECTRIC DISKS.

and shorted neighbor (Type D) have interface modes.

The electroacoustic transistor requires at least two interface states where an input acoustic wave propagates through one topological channel (referred to as the gate channel) which results in switching on or off a second channel (referred to as the output channel). It is ideal to use the same type of interface for both gate and output channels such that the wave speed in both channels is approximately the same while operating the transistor at a single frequency. However, due to the geometry of the system, the combination of two sublattices consisting of the same type of interface results in a third interface of a different type. Here, we exploit the absence of topological states in the Type A interface. We construct a transistor supercell by combining two sublattices containing Type D interfaces resulting in a third Type A interface at their junction. Repeating the eigenvalue computation for the transistor supercell produces the band structure shown in Fig. 4(a) for the ON (left) and OFF (right) configurations. Since the Type A interface does not host any topological states in the gap, the only interface states are those corresponding to energy localization in the gate and output channel. The different interfaces in the ON and OFF configuration are marked in Fig. 4(b) and (c), respectively, along with the displacement fields in the structure for a frequency in the gap. Reconfiguring the electrical connection of the piezoelectric disks in the dashed region in Fig. 4(b) and (c) from shunted to shorted, and vice versa, switches the output channel on and off. Next, we present an electrical circuit which reconfigures the system based on the amplitude of incoming acoustic signal.

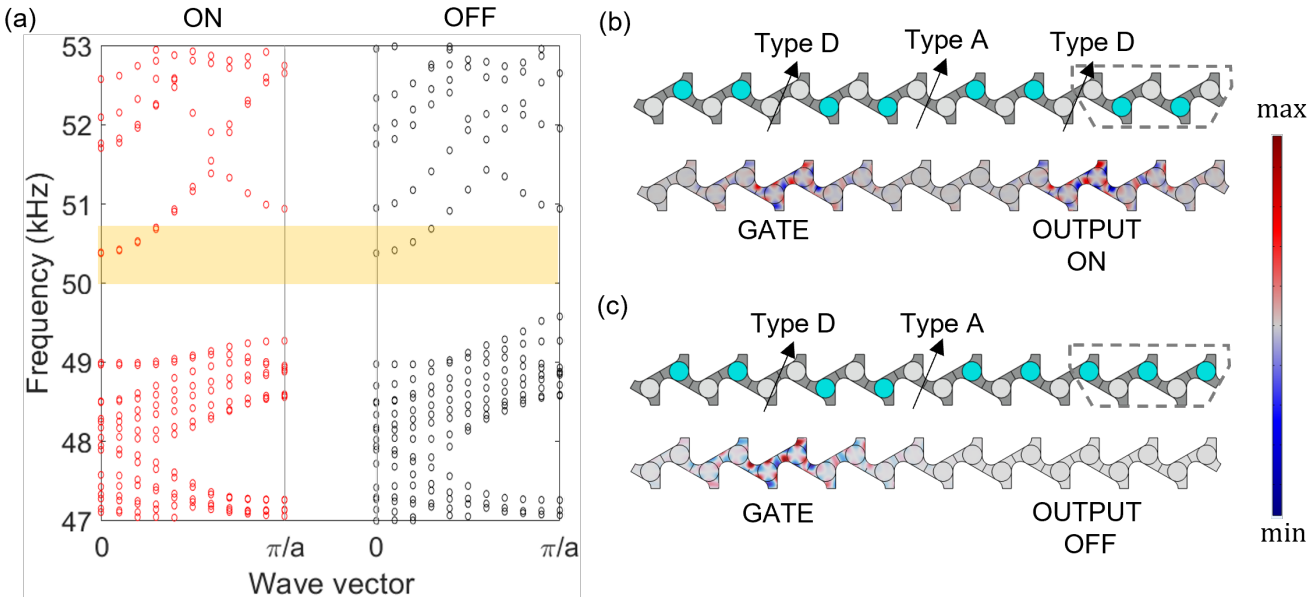

FIGURE 4. (a) BAND STRUCTURE OF THE TRANSISTOR SUPERCELL. HIGHLIGHTED FREQUENCY RANGE CONTAINS ONLY THE TOPOLOGICAL INTERFACE MODES. CONFIGURATION OF THE PIEZOS (TOP) AND CORRESPONDING MODE SHAPE (BOTTOM) WITHIN THE MARKED FREQUENCY REGION FOR (b) ON STATE and (c) OFF STATE OF THE TRANSISTOR.

SWITCHING THE TOPOLOGICAL CHANNEL

For detecting an incoming wave and switching the output channel, an electrical circuit shown in Fig. 5(a) is used which employs simple sub-circuits with operational amplifiers (OA1-4). One of the piezos in the gate channel is used to generate a voltage which corresponds to the input wave amplitude. This oscillating voltage signal (V_{in}) is processed to generate a DC voltage level which triggers relays to switch the electrical connections of the piezoelectric disks in the dashed region in Fig. 4(b) and (c). First a low charge oscillation from the piezoelectric disk is converted to a voltage (marked V_1 in the circuit) by OA1. OA2 and OA3 rectify the oscillating voltage V_1 and produce a DC signal of voltage V_3. OA4 provides any necessary gain to bring the voltage level to the input range of the relays used for reconfiguring the system. For the specific implementation shown in Fig. 5(b), a Texas Instruments LM324 chip is used which has four operational amplifiers built-in. A Metal Oxide Semiconductor FET (MOSFET) is additionally used at the output of OA4 to provide enough current to actuate the relay. The combination of OA4 and MOSFET could be replaced by a high current output operational amplifier which could drive the relays. Figure 5(c) depicts the experimentally measured voltages at the output of OA4 (V_{out}) for small variation in the voltage V_1. Clearly, the circuit is sensitive to small changes in the incoming acoustic signal as the output voltage changes by almost 2 V for less than 250 mV change in the peak amplitude of input signal. The gain provided by OA4 can be made tunable by replacing the resistance in the feedback loop of the amplifier with a variable resistor or potentiometer. This provides a control on the threshold setting of the input acoustic wave amplitude which switches the transistor state, allowing for application specific calibration of the device.

MODAL RESPONSE OF THE TRANSISTOR

The analysis conducted thus far involves an assumption of infinitely periodic media in at least one lattice vector direction. It is important to consider finite size effects to verify the functionality of the proposed device. To this end, we consider a finite structure with 6 transistor supercells of 10 unit cells each and study its harmonic response in the frequency range of 50 kHz to 51.5 kHz. Figure 6(a) depicts the frequency response of the structure computed at locations in the gate and output channels. The displacement is normalized with respect to the maximum response found at 50.7 kHz which is within the topological gap highlighted in yellow. The displacement field corresponding to the peak response in the gap is displayed in Fig. 6(b) and (c) for ON and OFF states, respectively. The harmonic response suggests that the reconfigurable structure hosts two distinct modes at the same frequency, one with and the other without a standing wave mode in the output channel, thus distinguishing the ON and OFF states. Wave propagation studies in the finite structure with disorder and experimental validation of the electroacoustic transistor are ongoing.

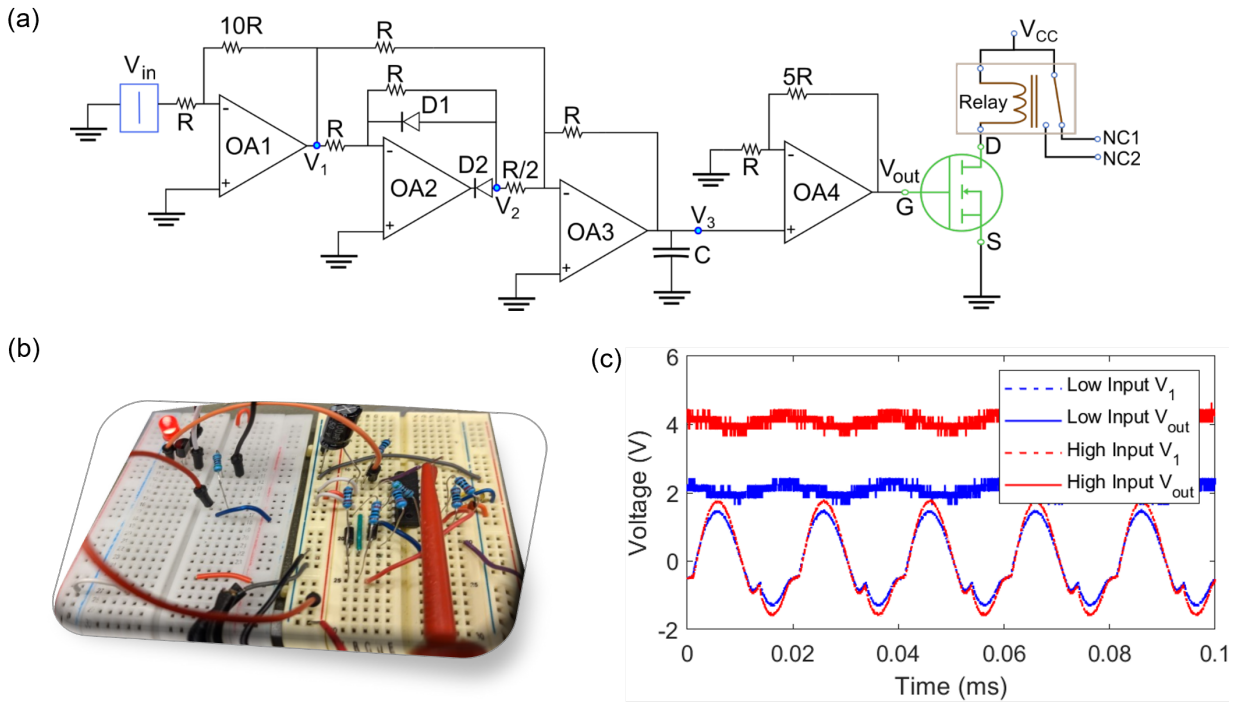

FIGURE 5. (a) ELECTRICAL CIRCUIT TO CONTROL SWITCHING OF THE TOPOLOGICAL STATE BETWEEN SOURCE AND DRAIN. (b) A MOCK-UP OF THE PROPOSED CIRCUIT (C) EXPERIMENTALLY MEASURED VOLTAGES IN THE SWITCHING CIRCUIT FOR TWO DIFFERENT (LOW AND HIGH) WAVE INPUTS TO THE TRANSISTOR STRUCTURE. V_1 AND V_{out} ARE VOLTAGES AT NODES MARKED IN (a)

CONCLUDING REMARKS

In summary, we designed an electroacoustic transistor in which wave transport occurs between a wave source and receiver depending on the amplitude of an incoming wave at a gate location. The transistor has a hexagonal lattice structure with a reconfigurable unit cell composed of piezoelectric attachments which are selectively shunted to enable the desired functioning of the device. We used finite element analysis to study the eigenvalues and harmonic response of the unit cell and finite structure, respectively, to demonstrate the ON and OFF states of the transistor where waves propagate through topologically-protected channels. Further, we prototyped an electrical circuit to enable switching on and off the output topological channel based on the amplitude of incoming wave in the gate channel. This work outlines a design procedure for the electroacoustic transistor based on topological insulators. The topological protection in the proposed transistor enables robust wave propagation and ensures stable output states even in the presence of defects or disorder. Multiple transistors can be connected through conventional elastic waveguides to produce logic gates. The device holds promise for hybrid computing technologies which combine electronic and acoustic wave-based signals. It is suitable for use in extreme or harsh environments and may be adapted to find potential applications in edge computing, communication and sensor technology.

ACKNOWLEDGEMENTS

This material is based upon work supported by the National Science Foundation under Grant 1929849. Any opinions, findings, and conclusions or recommendations expressed in this material are those of the author(s) and do not necessarily reflect the views of the National Science Foundation.

REFERENCES

[1] Yasuda, H., Buskohl, P. R., Gillman, A., Murphey, T. D., Stepney, S., Vaia, R. A., and Raney, J. R., 2021. "Mechanical computing". *Nature,* ***598***(7879), pp. 39–48.

[2] Qian, G., Lu, S., Pan, D., Tang, H., Liu, Y., and Wang, Q., 2019. "Edge computing: A promising framework for real-time fault diagnosis and dynamic control of rotating machines using multi-sensor data". *IEEE Sensors Journal,* ***19***(11), pp. 4211–4220.

[3] Zhou, L., and Wang, F., 2021. "Edge computing and ma-

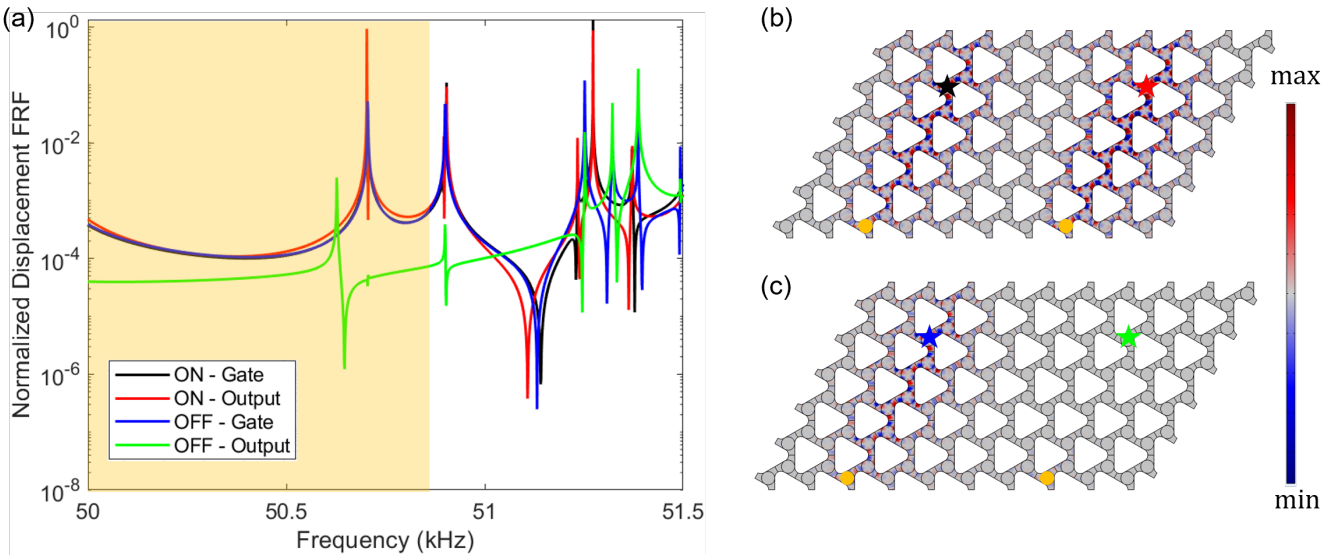

FIGURE 6. (a) FREQUENCY RESPONSE OF TRANSISTOR STRUCTURE MEASURED IN THE TWO TOPOLOGICAL CHANNELS. THE TOPOLOGICAL BANDGAP IS MARKED (b) DISPLACEMENT FIELD ACROSS THE STRUCTURE CORRESPONDING TO THE PEAK FREQUENCY IN THE TOPOLOGICAL GAP SHOWN IN (a). CIRCLES AND STARS INDICATE THE ACOUSTIC SOURCE AND RESPONSE LOCATIONS, RESPECTIVELY.

chinery automation application for intelligent manufacturing equipment". *Microprocessors and Microsystems,* ***87***, p. 104389.

[4] Raney, J. R., Nadkarni, N., Daraio, C., Kochmann, D. M., Lewis, J. A., and Bertoldi, K., 2016. "Stable propagation of mechanical signals in soft media using stored elastic energy". *Proceedings of the National Academy of Sciences,* ***113***(35), pp. 9722–9727.

[5] Jiang, Y., Korpas, L. M., and Raney, J. R., 2019. "Bifurcation-based embodied logic and autonomous actuation". *Nature communications,* ***10***(1), p. 128.

[6] Chen, T., Pauly, M., and Reis, P. M., 2021. "A reprogrammable mechanical metamaterial with stable memory". *Nature,* ***589***(7842), pp. 386–390.

[7] Waheed, U., Myant, C., and Dobson, S., 2020. "Boolean and/or mechanical logic using multi-plane mechanical metamaterials". *Extreme Mechanics Letters,* ***40***, p. 100865.

[8] El Helou, C., Grossmann, B., Tabor, C. E., Buskohl, P. R., and Harne, R. L., 2022. "Mechanical integrated circuit materials". *Nature,* ***608***(7924), pp. 699–703.

[9] El Helou, C., Buskohl, P. R., Tabor, C. E., and Harne, R. L., 2021. "Digital logic gates in soft, conductive mechanical metamaterials". *Nature communications,* ***12***(1), p. 1633.

[10] Song, Y., Panas, R. M., Chizari, S., Shaw, L. A., Jackson, J. A., Hopkins, J. B., and Pascall, A. J., 2019. "Additively manufacturable micro-mechanical logic gates". *Nature communications,* ***10***(1), p. 882.

[11] Ilyas, S., and Younis, M. I., 2020. "Resonator-based m/nems logic devices: Review of recent advances". *Sensors and Actuators A: Physical,* ***302***, p. 111821.

[12] Wang, Y., Xia, J.-p., Sun, H.-x., Yuan, S.-q., and Liu, X.-j., 2019. "Binary-phase acoustic passive logic gates". *Scientific Reports,* ***9***(1), p. 8355.

[13] Zhang, T., Cheng, Y., Guo, J.-z., Xu, J.-y., and Liu, X.-j., 2015. "Acoustic logic gates and boolean operation based on self-collimating acoustic beams". *Applied Physics Letters,* ***106***(11), p. 113503.

[14] Zhang, T., Cheng, Y., Yuan, B.-G., Guo, J.-Z., and Liu, X.-J., 2016. "Compact transformable acoustic logic gates for broadband complex boolean operations based on density-near-zero metamaterials". *Applied Physics Letters,* ***108***(18), p. 183508.

[15] Li, F., Anzel, P., Yang, J., Kevrekidis, P. G., and Daraio, C., 2014. "Granular acoustic switches and logic elements". *Nature communications,* ***5***(1), p. 5311.

[16] Ding, J., Wang, X., Gu, L., Li, S., Luo, X., Zhao, C., and Huang, Z., 2021. "Continuous and rapid sound regulation via a compact linear electroacoustic field effect transistor". *Physical Review Research,* ***3***(4), p. 043206.

[17] Sugino, C., Leadenham, S., Ruzzene, M., and Erturk, A., 2017. "An investigation of electroelastic bandgap formation in locally resonant piezoelectric metastructures". *Smart Materials and Structures,* ***26***(5), p. 055029.

[18] Allam, A., Elsabbagh, A., and Akl, W., 2017. "Experimental demonstration of one-dimensional active plate-type acoustic metamaterial with adaptive programmable density". *Journal of Applied Physics,* ***121***(12), p. 125106.

[19] Lu, L., Joannopoulos, J. D., and Soljačić, M., 2014. "Topological photonics". *Nature Photonics,* ***8***(11), p. 821.

[20] Hasan, M. Z., and Kane, C. L., 2010. "Colloquium: topological insulators". *Reviews of modern physics,* ***82***(4), p. 3045.

[21] Khanikaev, A. B., Hossein Mousavi, S., Tse, W.-K., Kargarian, M., MacDonald, A. H., and Shvets, G., 2013. "Photonic topological insulators". *Nature materials,* ***12***(3), pp. 233–239.

[22] Wang, Z., Chong, Y., Joannopoulos, J. D., and Soljačić, M., 2009. "Observation of unidirectional backscattering-immune topological electromagnetic states". *Nature,* ***461***(7265), pp. 772–775.

[23] Fleury, R., Sounas, D. L., Sieck, C. F., Haberman, M. R., and Alù, A., 2014. "Sound isolation and giant linear nonreciprocity in a compact acoustic circulator". *Science,* ***343***(6170), pp. 516–519.

[24] Yang, Z., Gao, F., Shi, X., Lin, X., Gao, Z., Chong, Y., and Zhang, B., 2015. "Topological acoustics". *Physical review letters,* ***114***(11), p. 114301.

[25] He, C., Ni, X., Ge, H., Sun, X.-C., Chen, Y.-B., Lu, M.-H., Liu, X.-P., and Chen, Y.-F., 2016. "Acoustic topological insulator and robust one-way sound transport". *Nature Physics,* ***12***(12), p. 1124.

[26] Von Klitzing, K., 1986. "The quantized hall effect". *Reviews of Modern Physics,* ***58***(3), p. 519.

[27] Kane, C. L., and Mele, E. J., 2005. "Quantum spin hall effect in graphene". *Physical review letters,* ***95***(22), p. 226801.

[28] Mak, K. F., McGill, K. L., Park, J., and McEuen, P. L., 2014. "The valley hall effect in mos2 transistors". *Science,* ***344***(6191), pp. 1489–1492.

[29] Rycerz, A., Tworzydo, J., and Beenakker, C., 2007. "Valley filter and valley valve in graphene". *Nature Physics,* ***3***(3), p. 172.

[30] Sui, M., Chen, G., Ma, L., Shan, W.-Y., Tian, D., Watanabe, K., Taniguchi, T., Jin, X., Yao, W., Xiao, D., and Zhang, Y., 2015. "Gate-tunable topological valley transport in bilayer graphene". *Nature Physics,* ***11***(12), p. 1027.

[31] Ma, T., and Shvets, G., 2016. "All-si valley-hall photonic topological insulator". *New Journal of Physics,* ***18***(2), p. 025012.

[32] Xiao, M., Chen, W.-J., He, W.-Y., and Chan, C. T., 2015. "Synthetic gauge flux and weyl points in acoustic systems". *Nature Physics,* ***11***(11), p. 920.

[33] Liu, T.-W., and Semperlotti, F., 2018. "Tunable acoustic valley–hall edge states in reconfigurable phononic elastic waveguides". *Physical Review Applied,* ***9***(1), p. 014001.

[34] Vila, J., Pal, R. K., and Ruzzene, M., 2017. "Observation of topological valley modes in an elastic hexagonal lattice". *Physical Review B,* ***96***(13), p. 134307.

[35] Wang, Z., Yang, Y., Li, H., Jia, H., Luo, J., Huang, J., Wang, Z., Jiang, B., Yang, N., Jin, G., et al., 2021. "Multichannel topological transport in an acoustic valley hall insulator". *Physical Review Applied,* ***15***(2), p. 024019.

[36] Darabi, A., Collet, M., and Leamy, M. J., 2020. "Experimental realization of a reconfigurable electroacoustic topological insulator". *Proceedings of the National Academy of Sciences,* ***117***(28), pp. 16138–16142.

[37] Yan, M., Lu, J., Li, F., Deng, W., Huang, X., Ma, J., and Liu, Z., 2018. "On-chip valley topological materials for elastic wave manipulation". *Nature Materials,* ***17***(11), pp. 993–998.

[38] Darabi, A., Kliewer, E., and Leamy, M. J., 2021. "Reconfigurable acoustic multiplexer/demultiplexer using time division". *Applied Physics Letters,* ***119***(11), p. 113501.

[39] Ma, J., Sun, K., and Gonella, S., 2019. "Valley hall in-plane edge states as building blocks for elastodynamic logic circuits". *Physical Review Applied,* ***12***(4), p. 044015.

[40] Forward, R. L., 1979. "Electronic damping of vibrations in optical structures". *Applied optics,* ***18***(5), pp. 690–697.

[41] Hagood, N. W., and Von Flotow, A., 1991. "Damping of structural vibrations with piezoelectric materials and passive electrical networks". *Journal of sound and vibration,* ***146***(2), pp. 243–268.

[42] De Marneffe, B., and Preumont, A., 2008. "Vibration damping with negative capacitance shunts: theory and experiment". *Smart Materials and Structures,* ***17***(3), p. 035015.

[43] Date, M., Kutani, M., and Sakai, S., 2000. "Electrically controlled elasticity utilizing piezoelectric coupling". *Journal of Applied Physics,* ***87***(2), pp. 863–868.

[44] Chen, Y., Huang, G., and Sun, C., 2014. "Band gap control in an active elastic metamaterial with negative capacitance piezoelectric shunting". *Journal of Vibration and Acoustics,* ***136***(6).

[45] COMSOL Multiphysics®v. 6.0. `www.comsol.com`. COMSOL AB, Stockholm, Sweden.

[46] Gao, N., Qu, S., Si, L., Wang, J., and Chen, W., 2021. "Broadband topological valley transport of elastic wave in reconfigurable phononic crystal plate". *Applied Physics Letters,* ***118***(6), p. 063502.

[47] Orazbayev, B., and Fleury, R., 2019. "Quantitative robustness analysis of topological edge modes in c6 and valley-hall metamaterial waveguides". *Nanophotonics,* ***8***(8), pp. 1433–1441.